HHS Public Access

Author manuscript

J Chem Neuroanat. Author manuscript; available in PMC 2022 October 01.

Published in final edited form as:

J Chem Neuroanat. 2021 October ; 116: 101998. doi:10.1016/j.jchemneu.2021.101998.

Cholinergic boutons are closely associated with excitatory cells and four subtypes of inhibitory cells in the inferior colliculus

Nichole L Beebe[1,2], **Brett R Schofield**[1,2]

[1]Hearing Research Focus Group, Northeast Ohio Medical University, Rootstown, OH

[2]Brain Health Research Institute, Kent State University, Kent, OH

Abstract

Acetylcholine (ACh) is a neuromodulator that has been implicated in multiple roles across the brain, including the central auditory system, where it sets neuronal excitability and gain and affects plasticity. In the cerebral cortex, subtypes of GABAergic interneurons are modulated by ACh in a subtype-specific manner. Subtypes of GABAergic neurons have also begun to be described in the inferior colliculus (IC), a midbrain hub of the auditory system. Here, we used male and female mice (*Mus musculus*) that express fluorescent protein in cholinergic cells, axons, and boutons to look at the association between ACh and four subtypes of GABAergic IC cells that differ in their associations with extracellular markers, their soma sizes, and their distribution within the IC. We found that most IC cells, including excitatory and inhibitory cells, have cholinergic boutons closely associated with their somas and proximal dendrites. We also found that similar proportions of each of four subtypes of GABAergic cells are closely associated with cholinergic boutons. Whether the different types of GABAergic cells in the IC are differentially regulated remains unclear, as the response of cells to ACh is dependent on which types of ACh receptors are present. Additionally, this study confirms the presence of these four subtypes of GABAergic cells in the mouse IC, as they had previously been identified only in guinea pigs. These results suggest that cholinergic projections to the IC modulate auditory processing via direct effects on a multitude of inhibitory circuits.

Corresponding author: Brett R. Schofield Department of Anatomy and Neurobiology Hearing Research Group Northeast Ohio Medical University Rootstown, OH 44272 USA. bschofie@neomed.edu.

CRediT Author Statement

Nichole Beebe: Conceptualization, Methodology, Formal Analysis, Investigation, Writing – Original Draft, Writing – Review & Editing, Visualization, **Brett Schofield:** Conceptualization, Methodology, Writing – Original Draft, Writing – Review & Editing, Visualization, Supervision, Funding Acquisition

Ethical Statement

The authors declare that the research was conducted in the absence of any commercial or financial relationships that could be construed as a potential conflict of interest.

Declaration of Interest

None.

Keywords

Acetylcholine; Perineuronal Net; VGLUT2; Mouse

1. Introduction[1]

Acetylcholine (ACh) modulates central auditory processing and has been implicated in temporal acuity, neuronal excitability and gain, plasticity and perception in a noisy environment (Felix, Chavez, Novicio, Morley, & Portfors, 2019; Gil & Metherate, 2019; Ison & Bowen, 2000; Kuenzel, 2019; Luo, Liu, Wang, & Yan, 2011; Schofield & Hurley, 2018; Sottile et al. 2017). ACh is prominent in the inferior colliculus (IC), a midbrain hub for both ascending and descending auditory pathways. Nicotinic and muscarinic cholinergic receptors are present throughout the IC and ACh modulates the responses to acoustic stimuli of a majority of IC cells (Farley, Morley, Javel, & Gorga, 1983; Glendenning & Baker, 1988; Habbicht & Vater, 1996; Morley & Happe, 2000; Schwartz, 1986; Watanabe & Simada, 1973). A majority of the cholinergic inputs to the IC originate in the pontomesencephalic tegmentum (PMT), a prominent midbrain cholinergic group that innervates much of the auditory brainstem and thalamus (Schofield, Motts, & Mellott, 2011). Cholinergic projections from the PMT contact both glutamatergic and GABAergic cells in the IC, suggesting direct cholinergic effects on both excitatory and inhibitory midbrain circuits (Noftz, Beebe, Mellott, & Schofield, 2020).

In neocortex and hippocampus, identification of subtypes of inhibitory cells has helped to increase the understanding of neuromodulation (Kubota, 2014; Rudy, Fishell, Lee, & Hjerling-Leffler, 2011; Lovett-Barron & Losonczy, 2014). In these areas, ACh directly contacts multiple GABAergic subtypes, allowing for cholinergic modulation of different inhibitory circuits (Lawrence, 2008). To what extent do different GABAergic subtypes in the IC receive cholinergic input? Subtypes of inhibitory and excitatory IC cells have recently begun to be identified (Beebe, Young, Mellott, & Schofield, 2016; Geis & Borst, 2013; Goyer et al., 2019; Ito, Bishop, & Oliver, 2009; Schofield & Beebe, 2019; Silveira et al., 2020). In the IC of guinea pigs, GABAergic cells can be separated into four subtypes that differ in their soma size and distribution within the IC (Beebe, Young, Mellott, & Schofield, 2016). The subtypes are distinguished based on their association with two extracellular markers: aggregates of extracellular matrix known as perineuronal nets (PNs) and dense axosomatic input from terminals expressing vesicular glutamate transporter 2, or VGLUT2 rings.

Here, we used a transgenic mouse (*Mus musculus*) that expresses tdTomato in cholinergic cells and their axons to investigate cholinergic inputs to GABAergic and non-GABAergic cells in the mouse IC. In order to investigate cholinergic inputs to GABAergic subtypes, we first evaluated whether the four GABAergic subtypes previously identified in guinea pig are

[1]**Abbreviations:** ACh: acetylcholine; IC: inferior colliculus; ICc: central nucleus of the inferior colliculus; ICd: dorsal cortex of the inferior colliculus; IClc: lateral cortex of the inferior colliculus; ICrp: rostral pole of the inferior colliculus; ICt: intercollicular tegmentum; mRVLM: medial rostral ventrolateral medulla; NBIC: nucleus of the brachium of the inferior colliculus; NGS: normal goat serum; PBS: phosphate-buffered saline; PMT: pontomesencephalic tegmentum; PN: perineuronal net; VGLUT2: vesicular glutamate transporter 2; WFA: *Wisteria floribunda* agglutinin

also present in mouse; both PNs and VGLUT2 rings have been reported in mouse IC (Fader, Imaizumi, Yanagawa, & Lee, 2016; Geis & Borst, 2013), but their association has not been examined. We confirmed that all four GABAergic subtypes are present in mouse IC, and that their differences in soma size and distribution within the IC follow the same patterns described in guinea pigs. We also found cholinergic boutons in close apposition to the somas and proximal dendrites of many IC neurons, including presumptive excitatory cells as well as all four subtypes of GABAergic cells, suggesting direct cholinergic modulation of numerous excitatory and inhibitory circuits of the auditory midbrain.

2. Materials and Methods

2.1 Animals

All procedures are consistent with the National Institutes of Health Guide for Care and Use of Laboratory Animals and were approved by the Northeast Ohio Medical University Institutional Animal Care and Use Committee. Efforts were made to minimize pain and the number of animals needed for the study. Animals used were the offspring of *ChAT*^{Cre,Cdh23WT} mice, which express Cre recombinase under the *ChAT* promoter (in cholinergic cells) and carry the wild-type *Cdh23* allele (and therefore do not suffer the early-onset high frequency hearing loss associated with the C57BL/6J background; Beebe et al., 2020). *ChAT*^{Cre,Cdh23WT} mice were crossed with B6.Cg-*Gt(Rosa)26Sor*$^{tm14(CAG-tdTomato)Hze}$/J mice (*Ai14* reporter mice, The Jackson Laboratory, stock no. 007914) to produce ChAT^{Cre}-tdTomato mice that express tdTomato in cholinergic cells. The resulting mice were heterozygous for the wild-type *Cdh23* allele, and so would be expected to display normal audiograms throughout adulthood (Frisina et al., 2011). Data were collected from three mice (one female and two males) that ranged in age from four to five months.

2.2 Tissue Collection and Processing

Each animal was deeply anesthetized with isoflurane until breathing stopped and corneal and withdrawal reflexes were absent. The animal was then perfused transcardially with Tyrode's solution, followed by 50 ml of 4% paraformaldehyde in 0.1 M phosphate buffer, pH 7.4, then 50 ml of the same fixative containing 10% sucrose. The brain was removed and stored in fixative containing 25% sucrose at 4°C overnight. The following day, the brain was frozen and cut into 40 μm sections in the transverse plane on a sliding microtome. Sections were collected in three series.

For one series, sections were stained for GABAergic subtypes following a protocol similar to that used previously in guinea pigs (Beebe, Noftz, & Schofield, 2020; Beebe, Young, Mellott, & Schofield, 2016). Tissue sections were washed in phosphate-buffered saline (PBS; 0.9% NaCl in 0.01 M phosphate buffer, pH 7.4) and then permeabilized in 0.2% Triton X-100 in PBS for 30 minutes. Nonspecific staining was blocked by treating sections with 10% normal goat serum (NGS) and 0.1% Triton X-100 in PBS for one hour. After blocking, PNs were stained with biotinylated *Wisteria floribunda* agglutinin (WFA) in PBS for one hour (1:100; Vector Laboratories B-1355; RRID: AB_2336874). The WFA was labeled by incubating tissue in a solution of Alexa Fluor 405-conjugated streptavidin

(1:100; Molecular Probes S-32351) in PBS for one hour at room temperature. Sections were rinsed with PBS, and then a mixture of primary antibodies was applied in a solution containing 1% NGS and 0.2% Triton X-100. Sections were allowed to incubate at 4°C for 48 hours. The following antibodies were included in the mixture: anti-GAD67 to label GABAergic neurons (1:250; Millipore MAB5406; RRID: AB_2278725), anti-VGLUT2 to label VGLUT2-containing boutons (1:2500; Millipore AB2251; RRID: AB_2665454), anti-NeuN as a neuron-specific stain (1:500; Millipore ABN78; RRID: AB_10807945), and Neuro-Chrom pan-neuronal marker to help label the proximal processes of neurons (1:1000; Millipore ABN2300; RRID: AB_10953966). Sections were then incubated in a mixture including an Alexa Fluor 488-conjugated anti-mouse antibody (to reveal GAD67; 1:100; Molecular Probes A21202; RRID: AB_141607), an Alexa Fluor 750-conjugated anti-rabbit antibody (to reveal NeuN and Neuro-Chrom; 1:100; Molecular Probes A21039; RRID: AB_2535710), and an Alexa Fluor 647-conjugated anti-guinea pig antibody (to reveal VGLUT2; 1:100; Molecular Probes A21450; RRID: AB_2735091) in PBS. Sections were mounted on gelatin-coated slides from 0.2% gelatin solution, allowed to air dry, and then coverslipped with DPX mounting medium (Sigma).

To help distinguish IC subdivisions, a second series was stained using the same method, but the primary antibody cocktail included anti-GAD67 (1:250; Millipore MAB5406; RRID: AB_2278725) and anti-GlyT2 (1:2500; Synaptic Systems 272–004; RRID: AB_2619998). Primary antibodies were labeled with an Alexa Fluor 488-conjugated anti-mouse antibody (to reveal GAD67; 1:100; Molecular Probes A21202; RRID: AB_141607), and an Alexa Fluor 647-conjugated anti-guinea pig antibody (to reveal GlyT2; 1:100; Molecular Probes A21450; RRID: AB_2735091).

2.3 Antibody Characterization

WFA is a lectin stain that recognizes PNs across a wide variety of species and brain areas, including auditory brain areas (Sonntag, Blosa, Schmidt, Rübsamen, & Morawski, 2015). Staining in our results recognized extracellular structures with the distinctive appearance of PNs. This WFA stain was previously shown to stain structures also recognized by an antibody to aggrecan, a component of PNs (Beebe & Schofield, 2018).

The monoclonal antibody to GAD67 (MAB5406, used at 1:250) recognizes a recombinant form of the 67 kDa isoform of glutamic acid decarboxylase (GAD67). On a Western blot of mouse brain tissue, this antibody recognizes a single band at the appropriate molecular weight (Corder, et al., 2018). In our results, this antibody recognized a subset of cells stained with the NeuN/Neuro-Chrom cocktail, indicating staining of a subset of IC neurons, along with punctal staining of boutons, which is the expected pattern.

The VGLUT2 antiserum (AB2251, used at 1:2500) recognizes the C-terminal end sequence of the rat VGLUT2 protein. On a Western blot of mouse tissue, this antibody recognizes a single band at the appropriate molecular weight (Seigneur & Südhof, 2018). This antibody has also been shown to label terminals with excitatory morphology at the ultrastructural level (Zhang, et al., 2015). In our results this antibody stained boutons throughout the IC which were sometimes arranged as dense rings surrounding cell bodies, which is the expected staining pattern.

The NeuN antiserum (ABN78, used at 1:500) recognizes the N-terminal region of neuronal nuclear protein that ends at the start of the RNA recognition motif. On a Western blot of mouse brain tissue, this antibody recognizes multiple closely associated bands at the appropriate molecular weight (Chatterjee, et al., 2013). The Neuro-Chrom antiserum (ABN2300, used at 1:1000) is a polyclonal antibody blend that reacts against somatic, nuclear, dendritic, and axonal proteins specific to neurons. In our results, these two markers were visualized in the same fluorescent channel; however, when we visualized them in separate channels in preliminary experiments there was nearly complete overlap between the two, as would be expected for neuron-specific markers. Further, when compared to a fluorescent Nissl stain, both of these markers recognize cells with neuronal morphology but not those with glial morphology.

The GlyT2 antiserum (272–004, used at 1:2500) recognizes a recombinant protein corresponding to amino acids 1–229 of rat glycine transporter 2. On a Western blot of mouse spinal cord, this antibody recognizes a single band at the appropriate molecular weight (manufacturer's website). A previous study validated that this antibody recognizes glycinergic terminals in mouse spinal cord (Tulloch, Teo, Carvajal, Tessier-Lavigne, & Jaworski, 2019). In our results, this antibody recognized a subset of boutons throughout the IC, in the same distribution that has been reported previously (Choy Buentello, Bishop, & Oliver, 2015).

2.4 Data Analysis

Two transverse sections (one through the mid-rostro-caudal IC and one through the intercollicular region) were selected from each case. Each section was outlined using a Neurolucida reconstruction system (MBF Bioscience; RRID: SCR_001775) attached to a Zeiss AxioImager Z2 microscope. An adjacent section stained for GAD67 and GlyT2 was overlaid, and borders between the IC central nucleus (ICc), IC dorsal cortex (ICd), and IC lateral cortex (IClc) on the mid-rostro-caudal IC section were drawn as described by Choy Buentello, Bishop, & Oliver (2015). This process was identical to that used by Silveira et al. (2020), where photomicrographs of the staining are shown. Borders for the intercollicular regions (the rostral pole of the IC [ICrp], intercollicular tegmentum [ICt] and the nucleus of the brachium of the IC [NBIC]) were drawn using staining for GAD67 and WFA, as previously described in guinea pigs (Beebe, Noftz, & Schofield, 2020). While it is possible to distinguish two parts of the NBIC – a cell-rich core and a fiber-rich interstitial region – the number of GAD-staining cells in the interstitial region was low so we combined these regions into a single NBIC for analysis. A "virtual tissue" photomontage of NeuN immunoreactivity was collected at 1 μm-depth intervals with a 63X oil-immersion objective (numerical aperture 1.4). The montage was displayed on a Cintiq 21UX interactive pen display (Wacom) attached to the Neurolucida system. The section was outlined and then for each area of interest, the Cintiq stylus was used to manually trace the soma of every NeuN-reactive cell with a visible nucleolus within 4 μm of one cut surface of each section. We chose this depth as a criterion for analysis because preliminary analysis showed that each of the fluorescent markers penetrated the section at least this far; thus, lack of staining with a given marker is unlikely to be attributable to inadequate penetration of the staining reagents (Mellott, Foster, Ohl, & Schofield, 2014). The section outline, with its associated

NeuN-stained soma outlines, was then aligned to the original section, and each neuron was viewed with the appropriate fluorescence filters to identify expression of the stained markers (a PN, expression of GAD67, a dense ring of axosomatic VGLUT2-expressing boutons, or close association with tdTomato-labeled boutons). A soma was considered to have a dense ring of VGLUT2-expressing boutons if greater than approximately 75% of the perimeter was covered by VGLUT2+ puncta, a criterion set previously to guarantee consistency across studies (Beebe, Young, Mellott, & Schofield, 2016). A neuron was considered to have close association with cholinergic boutons if one or more tdTomato-labeled boutons was present in the same focal plane as a NeuN/Neuro-Chrom-labeled soma or proximal dendrite and there was no visible separation between the two structures. An image stack is shown in three planes in Figure 1, illustrating boutons that would (arrows) or would not (arrowheads) be considered in close apposition to a neuron for the purpose of our quantitative analysis. Each neuronal outline was color-coded to indicate the marker(s) with which it was associated (including GAD67 immunostaining, VGLUT2 rings and PNs, as well as close apposition with cholinergic boutons). A total of 2273 neurons were outlined and coded. Data including each cell's location (e.g., ICc), coded cell type (e.g., GAD67+), perimeter, area, X and Y coordinates of the centroid, and minimum and maximum Feret diameters for each soma outline were exported from Neurolucida into R v3.4.1 for Mac OS X (R Core Team, 2017) for all further analyses. Neurons with a profile that overlapped a subdivision outline were excluded from analysis, so as not to be counted twice.

The difference in average soma profile area between types of cells was tested with a linear mixed effects model. Animal number was included as a random factor in models to account for minor variations in soma size that could result from fixation differences. The "nlme" package was used for fitting of linear mixed effects models (Pinheiro, Bates, DebRoy, Sarkar, & R Core Team, 2017), and the "emmeans" package was used for pairwise comparisons (Tukey's HSD; Lenth, 2018). Because soma profile area data were log-normally distributed, data were log-transformed before statistical testing. Because only three cases were analyzed, a non-parametric Kruskal-Wallis test was used to compare the percentage of neurons receiving cholinergic contacts between subdivisions and intercollicular areas, between GAD+ and GAD-negative cells, and between GAD+ subtypes. Kruskal-Wallis tests were run in R. Composite plots and box plots were generated in R (for a detailed explanation of the generation of composite plots see Beebe, Young, Mellott, & Schofield, 2016). Bar graphs were generated in Microsoft Excel.

Photomicrographs were taken using a Zeiss AxioImager Z2 microscope with an attached Apotome II (Zeiss) using Neurolucida software (MBF Biosciences). Photographs were taken using structured illumination microscopy with optical sectioning at 0.5 μm depth intervals. Stacks varied in total thickness, as care was taken to include only the cell(s) which were the subject of the photomicrograph; this decreased both out-of-focus light within the frame and the chance that additional boutons would be included at focal depths outside the area of interest. Stacks ranged in total thickness from 3 μm to 8 μm, with an average thickness of 4.6 μm. Images shown are maximum intensity projections of collected stacks. Adobe Photoshop (CS6 and 2020, Adobe Systems) was used to add scale bars, and to crop and colorize images. Brightness and contrast levels were adjusted globally when necessary.

3. Results

3.1 Four subtypes of GABAergic cells are distinguishable in mouse IC

Subtyping of GAD+ IC cells based on their association with PNs and VGLUT2 rings has previously been described only in guinea pigs, so we first examined whether all four subtypes are present in the mouse IC and intercollicular regions. We found examples of all four subtypes of GAD+ cells in mouse IC (Figure 2), including GAD+ cells lacking both a PN and a ring of axosomatic VGLUT2+ terminals (GAD Only, white arrows in top row), GAD+ cells surrounded by a PN, but not a ring of VGLUT2+ terminals (GAD-PN, white arrows in second row), GAD+ cells surrounded by a ring of VGLUT2+ terminals, but not a PN (GAD-VGLUT2 ring, white arrow in third row), and GAD+ cells surrounded by both a PN and a ring of VGLUT2+ terminals (GAD-PN-VGLUT2 ring, white arrow in bottom row).

In guinea pig IC, these four subtypes of cells differ in their average soma size and in their distribution within the IC (Beebe, Young, Mellott, & Schofield, 2016). Similar patterns are true in the mouse IC. Figure 3A shows a boxplot depicting the medians and ranges of soma profile areas for GAD-negative cells, as well as three of the four subtypes of GAD+ cells (The GAD-VGLUT2 ring group was too small for statistical comparison). On average, GAD-negative cells had the smallest soma sizes (mean of 72 μm^2), followed by GAD Only cells (85 μm^2) and GAD-PN cells (110 μm^2), with GAD-PN-VGLUT2 ring cells having the largest soma average soma size (150 μm^2). Across four GAD-VGLUT2 ring cells, the average soma size was 136 μm^2. A linear mixed effects model of the data (not including the GAD-VGLUT2 ring group) was constructed, and a likelihood ratio test showed that there was a significant relationship between soma profile area and GAD subtype ($\chi^2_{(3)} = 230.43$, $p < 0.001$). Pairwise comparison using a Tukey's HSD test showed significant differences in mean soma profile area between the GAD-negative and each GAD+ group ($p = 0.002$ for GAD-negative-GAD Only comparison and $p < 0.0001$ for all other comparisons), between the GAD Only and GAD-PN groups ($p < 0.0001$), between the GAD Only and GAD-PN-VGLUT2 ring groups ($p < 0.0001$), and between the GAD-PN and GAD-PN-VGLUT2 ring groups ($p < 0.0001$).

The four subtypes of GAD+ cells also differ in their distribution within the IC subdivisions and intercollicular regions. Figure 3B shows the proportions of GAD subtypes in each of the regions examined. GAD Only cells were the most prevalent GAD+ subtype in the ICd and ICt, while GAD-PN cells were the most prevalent subtype in the ICc, ICrp, and NBIC. GAD Only and GAD-PN cells made up very similar proportions of the GAD+ population in the IClc.

3.2 Most cells in mouse IC are in close association with cholinergic boutons

In the IC of $ChAT^{Cre}$-tdTomato mice, many tdTomato-labeled (cholinergic) axons were present across the IC. Both en passant and terminal boutons were readily identified. We combined staining for NeuN and Neuro-Chrom to label neurons and their proximal processes, and we found many examples of cholinergic boutons in close association with neurons and proximal dendrites in each area examined (Figure 4A, arrows). Neurons

typically had one to five presumptive cholinergic contacts. Lack of staining of distal dendrites prevented us from seeing any contacts on these processes, but the presence of many boutons in the neuropil suggest that distal dendrites are also targeted. Thus, we assume that we are underestimating the number of neurons with close cholinergic associations, but we still found that in most areas the majority of neurons received presumptive cholinergic contacts (Figure 4B). There was no obvious difference in the percentage of neurons receiving cholinergic contacts between areas, and a Kruskal-Wallis test confirmed that there was no significant relationship between percentage of cells with cholinergic contacts and area ($\chi^2_{(6)} = 7.00$, $p = 0.32$).

Both GAD+ and GAD-negative neurons were observed to receive cholinergic contacts in each area. An example of a single field is shown in Figure 5A, where cholinergic axons (red) are in close association with both GAD+ (green arrows) and GAD-negative (yellow arrows) cells. Across three cases, the majority of both GAD+ and GAD-negative cells were in close association with cholinergic boutons (Figure 5B). There was no obvious difference in the percentage of neurons receiving cholinergic contacts between GAD+ and GAD-negative cells, and a Kruskal-Wallis test confirmed that there was no significant relationship between percentage of cells with cholinergic contacts and neurotransmitter phenotype ($\chi^2_{(1)} = 0.05$, $p = 0.83$).

3.3 All subtypes of GABAergic cells are in close association with cholinergic boutons

We observed many examples of close association between cholinergic boutons and the various subtypes of GAD+ cells (Figure 6). These apparent contacts were found throughout the IC subdivisions and the intercollicular regions examined. Contacts were observed on somas and on dendrites and, in some cases were adjacent to GAD+ boutons that also appeared to be contacting the GABAergic cell (e.g., Figure 6, inset in bottom row). There were no obvious differences between the subtypes in the number of contacts they received or in the percentage of each subtype that received presumptive cholinergic contacts (Figure 7). A Kruskal-Wallis test (excluding the GAD-VGLUT2 ring group due to its small sample size) confirmed that there was no significant relationship between percentage of cells with cholinergic contacts and GAD subtype ($\chi^2_{(2)} = 3.20$, $p = 0.20$).

4. Discussion

4.1 Conclusions

We investigated the association between cholinergic boutons and neurons in the mouse IC and intercollicular regions. First, we found that the four subtypes of GABAergic cells distinguished in guinea pig IC can also be distinguished in the mouse IC. The subtypes in mice exhibit soma sizes and spatial distributions across midbrain auditory areas similar to that described in guinea pigs (Beebe, Young, Mellott & Schofield, 2016; Beebe, Noftz & Schofield, 2020). We then found that cholinergic boutons form close associations with the majority of non-GABAergic cells, as well as with all four subtypes of GABAergic cells (Figure 8). Such associations were present throughout the collicular and intercollicular regions examined. These results suggest that ACh modulates excitatory circuits as well as

a variety of inhibitory circuits arising across multiple auditory processing regions of the midbrain.

4.2 Technical Considerations

An important consideration in any study of the auditory system that uses transgenic mice is the genotype of those mice, specifically whether they carry a point mutation in the *cdh23* gene known as the *ahl* mutation, present in the C57BL/6 strain (Noben-Trauth, Zheng, & Johnson, 2003). This mutation causes early onset high-frequency hearing loss and, likely, alterations in the central auditory system (Ohlemiller, Jones, & Johnson, 2016; Zheng, Johnson, & Erway, 1999). Mice that are heterozygous for this mutation have normal auditory brainstem response thresholds throughout their lifespans but display decreased temporal processing abilities after one year of age (Burghard, Morel, & Oliver, 2019; Frisina et al., 2011). The animals used here were well below one year of age and would therefore be expected to have normal auditory physiology.

It is possible that some of the close appositions we observed between cholinergic boutons and neurons (GABA+ or GABA-negative) did not form synaptic contacts. Anatomical tracing and electrophysiological studies suggest cholinergic input to neurons across the IC (e.g., Farley, Morley, Javel, & Gorga, 1983; Habbicht & Vater, 1996; Yigit, Keipert, & Backus, 2003; Motts & Schofield, 2009; Felix, Chavez, Novicio, Morley, & Portfors, 2019; Noftz, Beebe, Mellott & Schofield, 2020). In vitro physiology has provided further evidence for direct cholinergic activation of GABAergic IC cells (Yigit, Keipert, & Backus, 2003). Nonetheless, there is ongoing debate on whether cholinergic transmission throughout the nervous system is via traditional synapses or volume transmission; it appears likely that both modes exist (see reviews by Sarter and Lustig, 2020 and Disney and Higley, 2020). One mode may be more prevalent in a given area; e.g., synaptic transmission may be dominant in the spinal cord, with synapses onto somas and dendrites, whereas volume transmission may be more prominent in neocortex (see discussions in Descarries and Mechawar, 2008; Disney and Higley, 2020; Sarter and Lustig, 2020). Complicating this debate has been the demonstration of cholinergic synapses that lack a clear postsynaptic density (a criterion often used to distinguish synaptic vs. non-synaptic release; Takács, Freund and Nyiri, 2013). Further studies, including electron microscopy and in vitro physiology, are needed to address these issues in the IC. In any case, the close proximity of ACh release sites would support activation of nearby neurons that express ACh receptors. Given the presence of multiple types of ACh receptors and demonstrated physiological effects of ACh in the IC, we believe it is likely that the boutons on the cholinergic axons shown here represent sites of ACh release, and that the adjacent neurons are likely to be affected directly.

In addition to direct postsynaptic effects, there may be presynaptic effects of ACh on other synapses (not visualized in our tissue) arising from boutons adjacent to the cholinergic boutons. Such presynaptic effects have been documented in many locations, including on collicular axons that terminate in the thalamus (Sottile et al., 2017). If present in the IC or intercollicular regions, presynaptic effects could provide modulation selective for a specific subset of inputs to the targeted cell.

4.3 GABAergic subtypes across rodent species

One of the main findings here was that subtypes of GABAergic neurons previously described in guinea pigs are also present in mouse IC. Further, differences in soma size and in distribution of the subtypes within the IC in guinea pig are similar in mouse. As VGLUT2 rings are present in the IC in rats, and PNs have been observed in the IC of rats and naked mole rats, these GABAergic subtypes may be conserved across rodent species (Beebe & Schofield, 2018; Friauf, 2000; Ito, Bishop, & Oliver, 2009; Seeger, Brauer, Härtig, & Brückner, 1994). PNs have also been reported in the IC of dogs and rhesus (Atoji, Yamamoto, Suzuki, Matsui, & Oohira, 1997; Hilbig, Nowack, Boeckler, Bidmon, & Zilles, 2007), introducing the possibility that the GABAergic subtypes described here are conserved beyond rodents.

The functional implications of the GABAergic subtypes have been discussed extensively (Beebe, Young, Mellott, & Schofield, 2016; Schofield & Beebe, 2019). Heavy glutamatergic input onto GABAergic cells of the IC, which presumably emanates from the VGLUT2+ boutons of the VGLUT2 ring surrounding some GABAergic neurons, enables short latency GABAergic transmission from the IC to the medial geniculate body (Geis & Borst, 2013; Ito, Bishop, & Oliver, 2009; Peruzzi, Bartlett, Smith, & Oliver, 1997). PNs may play a variety of roles in the IC, including modulation of synaptic physiology, reduction of structural plasticity, or protection from oxidative stress (for review see Fawcett, Oohashi, & Pizzorusso, 2019). In the auditory system specifically, PNs are implicated in the support of temporal precision in both the superior olivary complex and the medial geniculate body (Balmer, 2016; Blosa et al., 2015; Quraishe, Newman, & Anderson, 2019). In mice in this study, and in guinea pigs in a previous study, most IC neurons that were surrounded by VGLUT2 rings were also surrounded by PNs, indicating a potential interaction between the two structures (Beebe, Young, Mellott, & Schofield, 2016). It is possible that PNs around VGLUT2-ringed cells function to decrease structural plasticity, thereby “locking in” the specialized synaptic structure (Corvetti & Rossi, 2005; de Vivo et al., 2013).

A limitation of this way of subtyping IC GABAergic cells is that it relies on extracellular markers that cannot easily be used to genetically manipulate groups of GABAergic cells. A recent study classified a distinct subtype of GABAergic projection neuron in the IC that expresses neuropeptide Y (Silveira et al, 2020). Looking at whether these neuropeptide Y cells are surrounded by VGLUT2 rings or PNs could help to genetically classify the GABAergic subtypes we’ve described here. Further, expression of other neuropeptides could be investigated in order to find ways to genetically manipulate these GABAergic subtypes and learn more about their potentially differential functions.

4.4 Cholinergic modulation of IC neurons and circuits

ACh does not directly affect spontaneous activity in most IC cells (Curtis & Koizumi, 1961). However, ACh can affect various aspects of sound-evoked IC processing. During development, activation of muscarinic receptors increases GABA release in the IC (Yigit, Keipert, & Backus, 2003). In adulthood, ACh can support plastic changes in best frequency, modulate stimulus-specific adaptation, and support temporal processing in the IC (Ayala & Malmierca, 2015; Felix, Chavez, Novicio, Morley, & Portfors, 2019; Suga, 2012; Xiong,

Zhang, & Yan, 2009). Differences in cholinergic effects are likely related to several factors, including the IC subdivision under consideration, the types of cholinergic receptors expressed by the target cell, and finally the source of the cholinergic input.

The IC comprises multiple subdivisions that contribute to different aspects of hearing (Calford and Aitkin, 1983; Rouiller, 1997). The present results were similar across subdivisions in that the ACh axons appeared to contact GAD-negative (likely glutamatergic) cells and each subtype of GABAergic cell present in each area. Projections from the PMT (the primary source of cholinergic inputs to the IC) terminate across all IC subdivisions; in fact, individual cholinergic axons can provide boutons to multiple IC subdivisions, suggesting concurrent release of ACh in different areas (Noftz et al., 2020). Two factors support the hypothesis of different roles for ACh in the different subdivisions. First, the GABA subtypes are distributed differently across subdivisions; e.g., GABAergic cells associated with PNs are much more common in the ICc than in surrounding regions. If cholinergic modulation varies according to GABA subtype, the overall effects will vary by IC subdivision. Second, IC subdivisions differ in the complement of cholinergic receptors they contain.

There are two cholinergic receptor classes: nicotinic receptors (nAChRs) and muscarinic receptors (mAChRs), each of which exist in multiple subtypes. nAChRs contain α and β subunits of various subtypes. For example, the α7 receptor is a homopentamer of α7 subunits, while the α4β2 receptor is a heteropentamer of α4 and β2 subunits. The subunit composition affects ligand-binding, calcium permeability, and kinetics, conferring major functional consequences of expression (Gharpure et al. ‘20). Muscarinic receptors occur in five subtypes (M1-M5) categorized in two groups with opposite physiological effects: M1, M3 and M5 are depolarizing whereas M2 and M4 are typically hyperpolarizing. Both ionotropic nicotinic receptors and G-protein-coupled muscarinic receptors are distributed throughout the IC. Many studies describe high levels of the nicotinic α7 subunit in the IC (Arimatsu, Seto, & Amano, 1978; Clarke, Schwartz, Paul, Pert, & Pert, 1985; Happe & Morley, 2004; Morley & Happe, 2000; Morley, Lorden, Brown, Kemp, & Bradley, 1977; Rogers, Myers, & Gahring, 2012). There is less information about other nicotinic subunits, but α3β4 nicotinic receptors are also present (Gahring, Persiyanov, & Rogers, 2004; Marks et al., 2002; Whiteaker, Jimenez, McIntosh, Collins, & Marks, 2000). In addition, α4 and β2 units are expressed by glutamatergic and GABAergic IC cells (Sottile et al., 2017). The IC also contains M2 and M3 subtypes of muscarinic receptors (Hamada et al., 2010; Levey, Kitt, Simonds, Price, & Brann, 1991; Spencer, Horváth, & Traber, 1986). M3 AChRs appear to underlie direct cholinergic activation of IC GABAergic cells (Yigit, Keipert, & Backus, 2003).Details of AChR subtype distribution in the IC is incomplete, but some differences between subdivisions are clear. For nicotinic receptors, α7 and β4 subunits are more prevalent in the ICc and α4 subunits are more prevalent in areas outside the ICc (Gahring, Persiyanov, & Rogers, 2004; Happe and Morley 04; Hunt and Schmidt, ‘78). For muscarinic receptors, M1 is distributed rather evenly whereas M2 and M3 are more prevalent in the areas outside ICc (Hamada et al., 2010; Levey et al., ‘91; Spencer et al., ‘86). Thus, nicotinic and muscarinic effects are likely to differ by IC subdivision.

Cholinergic projections to the IC arise from two sources. The major projection arises from cholinergic cells of the pontomesencephalic tegmentum (PMT, comprising the pedunculopontine tegmental nucleus and laterodorsal tegmental nucleus) and a second, much smaller projection arises from the medial rostral ventrolateral medulla (mRVLM; Motts & Schofield, 2009; Stornetta, Macon, Nguyen, Coates & Guyenet, 2013). The PMT is associated with arousal, reward, motor function, and attention, while the mRVLM is associated with respiratory and autonomic function (Guyenet, 2014; Mena-Segovia & Bolam, 2017; Sved, Ito, & Yajima, 2002). The rostral part of the mRVLM may be equivalent to the lateral paragigantocellular nucleus (LPGi), a component of the reticular formation with connections to multiple auditory nuclei (Andrezik et al., 1981; Kamiya et al., 1988; Bellintani-Guardia et al., 1996). To our knowledge, nothing is known about the auditory responses of LPGi cells or the extent to which single cells in this area could reflect both autonomic and auditory function. Nonetheless, it is likely that the projections from the mRVLM/LPGi to the IC serve different purposes from those of the PMT. Whether different ACh sources contact different GABAergic subtypes is an interesting topic for future study.

In the medial geniculate body, ACh elicits inward currents via nicotinic receptors on thalamic cells as well as exerting presynaptic effects on inputs, including GABAergic inputs from the IC and glutamatergic inputs from the auditory cortex (Sottile et al., 2017; Sottile, Ling, Cox, & Caspary, 2017). The postsynaptic effects increase the gain of the thalamic cells, enhancing their responses to acoustic stimuli. The presynaptic effects were observed on ascending (tectothalamic) GABAergic projections but not on tectothalamic glutamatergic projections; i.e., on inhibitory but not excitatory ascending pathways. ACh also modulated cortical effects on the thalamus, enhancing excitatory corticothalamic effects but having no effect on cortically-driven inhibition via projections from the thalamic reticular nucleus to the medial geniculate cells. The authors concluded that the differential actions of ACh on excitatory and inhibitory inputs to the thalamus improve signal detection and enhance hearing in a noisy environment. In the present study, we saw presumptive ACh inputs to all four subtypes of GABAergic cells. Each subtype participates in the IC-medial geniculate body projection, so it seems very likely that the tectothalamic pathway is modulated by ACh at the level of the IC in addition to the axo-axonic modulation reported within the MG (Beebe, Mellott, & Schofield, 2018; Sottile et al., 2017). Specific roles for the different subtypes, and the nature of their modulation by ACh, remains to be determined. Which other IC circuits are modulated by ACh? Given the widespread distribution of cholinergic boutons in the IC, seemingly any IC circuit could be affected by direct cholinergic input. IC cells have local projections within the IC, projections across the IC commissure to the contralateral IC, and ascending projections to the medial geniculate body (Calford & Aitkin, 1983; González-Hernández, Meyer, & Ferres-Torres, 1986; Saldaña & Merchán, 1992). Additionally, IC cells make descending projections to the superior olivary complex and cochlear nucleus, and projections to “non-auditory” areas, such as the superior colliculus and the periaqueductal gray (Appell & Behan, 1990; Caicedo & Herbert, 1993; Xiong et al., 2015). Ascending, descending, and commissural pathways originate from mostly separate groups of cells within the IC (Coomes & Schofield, 2004; Okoyama, Ohbayashi, Ito, & Harada, 2006), providing an opportunity for different levels of modulation of different output pathways. In hippocampus and neocortex, differential effects of ACh on subtypes

of GABAergic neurons are based on differences in receptor expression (Lawrence, 2008). Similarly, effects on individual IC circuits would be heavily dependent on the types of receptors present, so investigation of the ACh receptor subtypes expressed by different populations of IC cells (e.g. GABAergic subtypes, neurons participating in different pathways, etc.) is a logical next step for investigation.

Acknowledgments

We thank Colleen Sowick for expert technical assistance.

Funding

This work was supported by the National Institutes of Health [grant R01 DC004391].

References

Andrezik JA, Chan-Palay V, Palay SL, 1981. The nucleus paragigantocellularis lateralis in the rat. Demonstration of afferents by the retrograde transport of horseradish peroxidase. Anat Embryol (Berl)161, 373–90. [PubMed: 7247035]

Appell PP, & Behan M (1990). Sources of subcortical GABAergic projections to the superior colliculus in the cat. The Journal of Comparative Neurology, 302, 143–158. doi: 10.1002/cne.903020111 [PubMed: 2086611]

Arimatsu Y, Seto A, & Amano T (1978). Localization of α-bungarotoxin binding sites in mouse brain by light and electron microscopic autoradiography. Brain Research, 147, 165–169. doi: 10.1016/0006-8993(78)90782-5 [PubMed: 656911]

Atoji Y, Yamamoto Y, Suzuki Y, Matsui F, & Oohira A (1997). Immunohistochemical localization of neurocan in the lower auditory nuclei of the dog. Hearing Research, 110, 200–208. doi: 10.1016/S0378-5955(97)00079-8 [PubMed: 9282902]

Ayala YA, & Malmierca MS (2015). Cholinergic Modulation of Stimulus-Specific Adaptation in the Inferior Colliculus. Journal of Neuroscience, 35, 12261–12272. doi: 10.1523/JNEUROSCI.0909-15.2015 [PubMed: 26338336]

Balmer TS (2016). Perineuronal Nets Enhance the Excitability of Fast-Spiking Neurons. Eneuro, 3, ENEURO.0112–16.2016. doi: 10.1523/ENEURO.0112-16.2016

Beebe NL, Mellott JG, & Schofield BR (2018). Inhibitory Projections from the Inferior Colliculus to the Medial Geniculate body Originate from Four Subtypes of GABAergic Cells. Eneuro, 5, ENEURO.0406–18.2018. doi: 10.1523/ENEURO.0406-18.2018

Beebe NL, Noftz WA, & Schofield BR (2020). Perineuronal nets and subtypes of GABAergic cells differentiate auditory and multisensory nuclei in the intercollicular area of the midbrain. Journal of Comparative Neurology, 528, 2695–2707. doi: 10.1002/cne.24926

Beebe NL, & Schofield BR (2018). Perineuronal nets in subcortical auditory nuclei of four rodent species with differing hearing ranges. Journal of Comparative Neurology, 526, 972–989. doi: 10.1002/cne.24383

Beebe NL, Sowick CS, Kristaponyte I, Galazyuk AV, Vetter DE, Cox BC, & Schofield BR (2020). Generation of a ChAT mouse line without the early onset hearing loss typical of the C57BL/6J strain. Hearing Research, 388, 107896. doi: 10.1016/j.heares.2020.107896 [PubMed: 31982642]

Beebe NL, Young JW, Mellott JG, & Schofield BR (2016). Extracellular Molecular Markers and Soma Size of Inhibitory Neurons: Evidence for Four Subtypes of GABAergic Cells in the Inferior Colliculus. The Journal of Neuroscience, 36, 3988–3999. doi: 10.1523/JNEUROSCI.0217-16.2016 [PubMed: 27053206]

Bellintani-Guardia B, Schweizer M, Herbert H, 1996. Analysis of projections from the cochlear nucleus to the lateral paragigantocellular reticular nucleus in the rat. Cell Tissue Res283, 493–505. [PubMed: 8593678]

Blosa M, Sonntag M, Jäger C, Weigel S, Seeger J, Frischknecht R, … Morawski M (2015). The extracellular matrix molecule brevican is an integral component of the machinery mediating fast

synaptic transmission at the calyx of Held: Impact of brevican on synaptic transmission. The Journal of Physiology, 593, 4341–4360. doi: 10.1113/JP270849 [PubMed: 26223835]

Burghard AL, Morel NP, & Oliver DL (2019). Mice heterozygous for the Cdh23/Ahl1 mutation show age-related deficits in auditory temporal processing. Neurobiology of Aging, 81, 47–57. doi: 10.1016/j.neurobiolaging.2019.02.029 [PubMed: 31247458]

Caicedo A, & Herbert H (1993). Topography of descending projections from the inferior colliculus to auditory brainstem nuclei in the rat. The Journal of Comparative Neurology, 328, 377–392. doi: 10.1002/cne.903280305 [PubMed: 7680052]

Chatterjee S, Mizar P, Cassel R, Neidl R, Selvi BR, Mohankrishna DV, … Boutillier A-L (2013). A Novel Activator of CBP/p300 Acetyltransferases Promotes Neurogenesis and Extends Memory Duration in Adult Mice. Journal of Neuroscience, 33, 10698–10712. doi: 10.1523/JNEUROSCI.5772-12.2013 [PubMed: 23804093]

Choy Buentello D, Bishop DC, & Oliver DL (2015). Differential distribution of GABA and glycine terminals in the inferior colliculus of rat and mouse: GABA and Glycine in Inferior Colliculus. Journal of Comparative Neurology, 523, 2683–2697. doi: 10.1002/cne.23810

Clarke P, Schwartz R, Paul S, Pert C, & Pert A (1985). Nicotinic binding in rat brain: Autoradiographic comparison of [3H]acetylcholine, [3H]nicotine, and [125I]-alpha-bungarotoxin. The Journal of Neuroscience, 5, 1307–1315. doi: 10.1523/JNEUROSCI.05-05-01307.1985 [PubMed: 3998824]

Coomes DL, & Schofield BR (2004). Separate projections from the inferior colliculus to the cochlear nucleus and thalamus in guinea pigs. Hearing Research, 191, 67–78. doi: 10.1016/j.heares.2004.01.009 [PubMed: 15109706]

Corder KM, Cortes MA, Bartley AF, Lear SA, Lubin FD, & Dobrunz LE (2018). Prefrontal cortex-dependent innate behaviors are altered by selective knockdown of Gad1 in neuropeptide Y interneurons. PLOS ONE, 13(7), e0200809. doi: 10.1371/journal.pone.0200809 [PubMed: 30024942]

Corvetti L, & Rossi F (2005). Degradation of Chondroitin Sulfate Proteoglycans Induces Sprouting of Intact Purkinje Axons in the Cerebellum of the Adult Rat. Journal of Neuroscience, 25, 7150–7158. doi: 10.1523/JNEUROSCI.0683-05.2005 [PubMed: 16079397]

Curtis DR, & Koizumi K (1961). Chemical transmitter substances in brain stem of cat. Journal of Neurophysiology, 24, 80–90. [PubMed: 13718944]

de Vivo L, Landi S, Panniello M, Baroncelli L, Chierzi S, Mariotti L, … Ratto GM (2013). Extracellular matrix inhibits structural and functional plasticity of dendritic spines in the adult visual cortex. Nature Communications, 4, 1484. doi: 10.1038/ncomms2491

Disney AA, Higley MJ, (2020). Diverse Spatiotemporal Scales of Cholinergic Signaling in the Neocortex. J. Neurosci40, 720–725. 10.1523/JNEUROSCI.1306-19.2019 [PubMed: 31969490]

Fader S, Imaizumi K, Yanagawa Y, & Lee C (2016). Wisteria Floribunda Agglutinin-Labeled Perineuronal Nets in the Mouse Inferior Colliculus, Thalamic Reticular Nucleus and Auditory Cortex. Brain Sciences, 6, 13. doi: 10.3390/brainsci6020013

Farley GR, Morley BJ, Javel E, & Gorga MP (1983). Single-unit responses to cholinergic agents in the rat inferior colliculus. Hearing Research, 11, 73–91. doi: 10.1016/0378-5955(83)90046-1 [PubMed: 6309726]

Fawcett JW, Oohashi T, & Pizzorusso T (2019). The roles of perineuronal nets and the perinodal extracellular matrix in neuronal function. Nature Reviews Neuroscience, 20, 451–465. doi: 10.1038/s41583-019-0196-3 [PubMed: 31263252]

Felix RA, Chavez VA, Novicio DM, Morley BJ, & Portfors CV (2019). Nicotinic acetylcholine receptor subunit α_7 -knockout mice exhibit degraded auditory temporal processing. Journal of Neurophysiology, 122, 451–465. doi: 10.1152/jn.00170.2019 [PubMed: 31116647]

Friauf E (2000). Development of Chondroitin Sulfate Proteoglycans in the Central Auditory System of Rats Correlates with Acquisition of Mature Properties. Audiology and Neurotology, 5, 251–262. doi: 10.1159/000013889 [PubMed: 10899695]

Frisina RD, Singh A, Bak M, Bozorg S, Seth R, & Zhu X (2011). F1 (CBA×C57) mice show superior hearing in old age relative to their parental strains: Hybrid vigor or a new

animal model for “Golden Ears”? Neurobiology of Aging, 32, 1716–1724. doi: 10.1016/j.neurobiolaging.2009.09.009 [PubMed: 19879021]

Gahring LC, Persiyanov K, & Rogers SW (2004). Neuronal and astrocyte expression of nicotinic receptor subunit β4 in the adult mouse brain. Journal of Comparative Neurology, 468, 322–333. 10.1002/cne.10942

Geis HRAP, & Borst JGG (2013). Large GABAergic neurons form a distinct subclass within the mouse dorsal cortex of the inferior colliculus with respect to intrinsic properties, synaptic inputs, sound responses, and projections. Journal of Comparative Neurology, 521, 189–202. doi: 10.1002/cne.23170

Gharpure A, Noviello CM, Hibbs RE, (2020). Progress in nicotinic receptor structural biology. Neuropharmacology171, 108086. 10.1016/j.neuropharm.2020.108086 [PubMed: 32272141]

Gil SM, & Metherate R (2019). Enhanced sensory–cognitive processing by activation of nicotinic acetylcholine receptors. Nicotine & Tobacco Research, 21, 377–382. doi: 10.1093/ntr/nty134 [PubMed: 30137439]

Glendenning KK, & Baker BN (1988). Neuroanatomical distribution of receptors for three potential inhibitory neurotransmitters in the brainstem auditory nuclei of the cat. The Journal of Comparative Neurology, 275, 288–308. doi: 10.1002/cne.902750210 [PubMed: 2851616]

González-Hernández TH, Meyer G, & Ferres-Torres R (1986). The commissural interconnections of the inferior colliculus in the albino mouse. Brain Research, 368, 268–276. doi: 10.1016/0006-8993(86)90571-8 [PubMed: 2421840]

Goyer D, Silveira MA, George AP, Beebe NL, Edelbrock RM, Malinski PT, Schofield BR, Roberts MT, 2019. A novel class of inferior colliculus principal neurons labeled in vasoactive intestinal peptide-Cre mice 32. ELife, 8, e43770. doi: 10.7554/eLife.43770 [PubMed: 30998185]

Goyer D, Silveira MA, George AP, Beebe NL, Edelbrock RM, Malinski PT, … Roberts MT (2019). A novel class of inferior colliculus principal neurons labeled in vasoactive intestinal peptide-Cre mice.

Guyenet PG (2014). Regulation of Breathing and Autonomic Outflows by Chemoreceptors. In Terjung R (Ed.), Comprehensive Physiology (pp. 1511–1562). Hoboken, NJ, USA: John Wiley & Sons, Inc. doi: 10.1002/cphy.c140004

Habbicht H, & Vater M (1996). A microiontophoretic study of acetylcholine effects in the inferior colliculus of horseshoe bats: Implications for a modulatory role. Brain Research, 724, 169–179. doi: 10.1016/0006-8993(96)00224-7 [PubMed: 8828565]

Hamada S, Houtani T, Trifonov S, Kase M, Maruyama M, Shimizu J, Yamashita T, Tomoda K, & Sugimoto T (2010). Histological determination of the areas enriched in cholinergic terminals and M2 and M3 muscarinic receptors in the mouse central auditory system. Anatomical Record (Hoboken), 293(8), 1393–1399. 10.1002/ar.21186

Happe HK, & Morley BJ (2004). Distribution and postnatal development of α7 nicotinic acetylcholine receptors in the rodent lower auditory brainstem. Developmental Brain Research, 153(1), 29–37. doi: 10.1016/j.devbrainres.2004.07.004 [PubMed: 15464215]

Hilbig H, Nowack S, Boeckler K, Bidmon H-J, & Zilles K (2007). Characterization of neuronal subsets surrounded by perineuronal nets in the rhesus auditory brainstem. Journal of Anatomy, 210, 507–517. doi: 10.1111/j.1469-7580.2007.00713.x [PubMed: 17451528]

Hunt S, Schmidt J, (1978). Some observations on the binding patterns of alpha-bungarotoxin in the central nervous system of the rat. Brain research157, 213–32. [PubMed: 719523]

Ison JR, & Bowen GP (2000). Scopolamine reduces sensitivity to auditory gaps in the rat, suggesting a cholinergic contribution to temporal acuity. Hearing Research, 145, 169–176. doi: 10.1016/S0378-5955(00)00088-5 [PubMed: 10867290]

Ito T, Bishop DC, & Oliver DL (2009). Two Classes of GABAergic Neurons in the Inferior Colliculus. Journal of Neuroscience, 29, 13860–13869. doi: 10.1523/JNEUROSCI.3454-09.2009 [PubMed: 19889997]

Kamiya H, Itoh K, Yasui Y, Ino T, Mizuno N, 1988. Somatosensory and auditory relay nucleus in the rostral part of the ventrolateral medulla: a morphological study in the cat. J Comp Neurol273, 421–435. [PubMed: 2463282]

Kubota Y (2014). Untangling GABAergic wiring in the cortical microcircuit. Current Opinion in Neurobiology, 26, 7–14. doi: 10.1016/j.conb.2013.10.003 [PubMed: 24650498]

Kuenzel T (2019). Modulatory influences on time-coding neurons in the ventral cochlear nucleus. Hearing Research, 384, 107824. doi: 10.1016/j.heares.2019.107824 [PubMed: 31670183]

Lawrence JJ (2008). Cholinergic control of GABA release: Emerging parallels between neocortex and hippocampus. Trends in Neurosciences, 31, 317–327. doi: 10.1016/j.tins.2008.03.008 [PubMed: 18556072]

Lenth R (2018). emmeans: Estimated and marginal means, aka leastsquares means. R package version 1.1 URL: https://CRAN.Rproject.org/package_emmeans.

Levey A, Kitt C, Simonds W, Price D, & Brann M (1991). Identification and localization of muscarinic acetylcholine receptor proteins in brain with subtype-specific antibodies. The Journal of Neuroscience, 11, 3218–3226. doi: 10.1523/JNEUROSCI.11-10-03218.1991 [PubMed: 1941081]

Lovett-Barron M, & Losonczy A (2014). Behavioral consequences of GABAergic neuronal diversity. Current Opinion in Neurobiology, 26, 27–33. doi: 10.1016/j.conb.2013.11.002 [PubMed: 24650501]

Luo F, Liu X, Wang C, & Yan J (2011). The Pedunculopontine Tegmental Nucleus: A Second Cholinergic Source for Frequency-Specific Auditory Plasticity. Journal of Neurophysiology, 105, 107–116. doi: 10.1152/jn.00546.2010 [PubMed: 20980544]

Marks MJ, Whiteaker P, Grady SR, Picciotto MR, McIntosh JM, & Collins AC (2002). Characterization of [125I]epibatidine binding and nicotinic agonist-mediated 86Rb+ efflux in interpeduncular nucleus and inferior colliculus of β2 null mutant mice: Binding and function in β2 null mutants. Journal of Neurochemistry, 81, 1102–1115. doi: 10.1046/j.1471-4159.2002.00910.x [PubMed: 12065623]

Mellott JG, Foster NL, Ohl AP, & Schofield BR (2014). Excitatory and inhibitory projections in parallel pathways from the inferior colliculus to the auditory thalamus. Frontiers in Neuroanatomy, 8. doi: 10.3389/fnana.2014.00124

Mena-Segovia J, & Bolam JP (2017). Rethinking the Pedunculopontine Nucleus: From Cellular Organization to Function. Neuron, 94, 7–18. doi: 10.1016/j.neuron.2017.02.027 [PubMed: 28384477]

Morley BJ, & Happe HK (2000). Cholinergic receptors: Dual roles in transduction and plasticity. Hearing Research, 147, 104–112. doi: 10.1016/S0378-5955(00)00124-6 [PubMed: 10962177]

Morley BJ, Lorden JF, Brown GB, Kemp GE, & Bradley RJ (1977). Regional distribution of nicotinic acetylcholine receptor in rat brain. Brain Research, 134, 161–166. doi: 10.1016/0006-8993(77)90935-0 [PubMed: 912415]

Motts SD, & Schofield BR (2009). Sources of cholinergic input to the inferior colliculus. Neuroscience, 160, 103–114. doi: 10.1016/j.neuroscience.2009.02.036 [PubMed: 19281878]

Noben-Trauth K, Zheng QY, & Johnson KR (2003). Association of cadherin 23 with polygenic inheritance and genetic modification of sensorineural hearing loss. Nature Genetics, 35, 21–23. doi: 10.1038/ng1226

Noftz WA, Beebe NL, Mellott JG, & Schofield BR (2020). Cholinergic projections from the pedunculopontine tegmental nucleus contact excitatory and inhibitory neurons in the inferior colliculus. Frontiers in Neural Circuits, 14, 43. doi: 10.3389/fncir.2020.00043 [PubMed: 32765226]

Ohlemiller KK, Jones SM, & Johnson KR (2016). application of mouse models to research in hearing and balance. Journal of the Association for Research in Otolaryngology, 17, 493–523. doi: 10.1007/s10162-016-0589-1 [PubMed: 27752925]

Okoyama S, Ohbayashi M, Ito M, & Harada S (2006). Neuronal organization of the rat inferior colliculus participating in four major auditory pathways. Hearing Research, 218, 72–80. doi: 10.1016/j.heares.2006.04.004 [PubMed: 16814970]

Peruzzi D, Bartlett E, Smith PH, & Oliver DL (1997). A monosynaptic GABAergic input from the inferior colliculus to the medial geniculate body in rat. The Journal of Neuroscience, 17, 3766–3777. doi: 10.1523/JNEUROSCI.17-10-03766.1997 [PubMed: 9133396]

Pinheiro J, Bates D, DebRoy S, Sarkar D, & R Core Team (2017). Linear and nonlinear mixed effects models. R package version 3.1–131. URL: https://CRAN.R-project.org/package=nlme.

Quraishe S, Newman T, & Anderson L (2019). Auditory temporal acuity improves with age in the male mouse auditory thalamus: A role for perineuronal nets? Journal of Neuroscience Research, jnr.24537. doi: 10.1002/jnr.24537

R Core Team (2017) R: A language and environment for statistical computing. Vienna, Austria: R Foundation for Statistical Computing.

Rogers SW, Myers EJ, & Gahring LC (2012). The expression of nicotinic receptor alpha7 during cochlear development. Brain and Behavior, 2(5), 628–639. doi: 10.1002/brb3.84 [PubMed: 23139908]

Rouiller EM, (1997). Functional organization of the auditory pathways, in: Ehret G, Romand R (Eds.), The Central Auditory System. Oxford University Press, New York, pp. 3–96.

Rudy B, Fishell G, Lee S, & Hjerling-Leffler J (2011). Three groups of interneurons account for nearly 100% of neocortical GABAergic neurons. Developmental Neurobiology, 71, 45–61. doi: 10.1002/dneu.20853 [PubMed: 21154909]

Saldaña E, & Merchań MA (1992). Intrinsic and commissural connections of the rat inferior colliculus: INTRINSIC AND COMMISSURAL COLLICULAR CONNECTIONS. Journal of Comparative Neurology, 319, 417–437. doi: 10.1002/cne.903190308

Sarter M, Lustig C, (2020). Forebrain Cholinergic Signaling: Wired and Phasic, Not Tonic, and Causing Behavior. J. Neurosci40, 712–719. 10.1523/JNEUROSCI.1305-19.2019 [PubMed: 31969489]

Schofield BR, & Beebe NL (2019). Subtypes of GABAergic cells in the inferior colliculus. Hearing Research, 376, 1–10. doi: 10.1016/j.heares.2018.10.001 [PubMed: 30314930]

Schofield BR, & Hurley L (2018). Circuits for Modulation of Auditory Function. In Oliver DL, Cant NB, Fay RR, & Popper AN (Eds.), The Mammalian Auditory Pathways (Vol. 65, pp. 235–267). Cham: Springer International Publishing. doi: 10.1007/978-3-319-71798-2_9

Schofield BR, Motts SD, & Mellott JG (2011). Cholinergic cells of the pontomesencephalic tegmentum: Connections with auditory structures from cochlear nucleus to cortex. Hearing Research, 279, 85–95. doi: 10.1016/j.heares.2010.12.019 [PubMed: 21195150]

Schwartz RD (1986). Autoradiographic distribution of high affinity muscarinic and nicotinic cholinergic receptors labeled with [3H]acetylcholine in rat brain. Life Sciences, 38, 2111–2119. doi: 10.1016/0024-3205(86)90210-9 [PubMed: 3713440]

Seeger G, Brauer K, Härtig W, & Brückner G (1994). Mapping of perineuronal nets in the rat brain stained by colloidal iron hydroxide histochemistry and lectin cytochemistry. Neuroscience, 58, 371–388. doi: 10.1016/0306-4522(94)90044-2 [PubMed: 7512240]

Seigneur E, & Südhof TC (2018). Genetic Ablation of All Cerebellins Reveals Synapse Organizer Functions in Multiple Regions Throughout the Brain. The Journal of Neuroscience, 38, 4774–4790. doi: 10.1523/JNEUROSCI.0360-18.2018 [PubMed: 29691328]

Silveira MA, Anair JD, Beebe NL, Mirjalili P, Schofield BR, & Roberts MT (2020). Neuropeptide Y expression defines a novel class of GABAergic projection neuron in the inferior colliculus. The Journal of Neuroscience, JN-RM-0420–20. doi: 10.1523/JNEUROSCI.0420-20.2020

Sonntag M, Blosa M, Schmidt S, Rübsamen R, & Morawski M (2015). Perineuronal nets in the auditory system. Hearing Research, 329, 21–32. doi: 10.1016/j.heares.2014.12.012 [PubMed: 25580005]

Sottile SY, Hackett TA, Cai R, Ling L, Llano DA, & Caspary DM (2017). Presynaptic Neuronal Nicotinic Receptors Differentially Shape Select Inputs to Auditory Thalamus and Are Negatively Impacted by Aging. The Journal of Neuroscience, 37, 11377–11389. doi: 10.1523/JNEUROSCI.1795-17.2017 [PubMed: 29061702]

Sottile SY, Ling L, Cox BC, & Caspary DM (2017). Impact of ageing on postsynaptic neuronal nicotinic neurotransmission in auditory thalamus: Ageing and postsynaptic neuronal nicotinic neurotransmission. The Journal of Physiology, 595, 5375–5385. doi: 10.1113/JP274467 [PubMed: 28585699]

Spencer DG, Horváth E, & Traber J (1986). Direct autoradiographic determination of M1 and M2 muscarinic acetylcholine receptor distribution in the rat brain: Relation to cholinergic nuclei and projections. Brain Research, 380, 59–68. doi: 10.1016/0006-8993(86)91429-0 [PubMed: 3756473]

Stornetta RL, Macon CJ, Nguyen TM, Coates MB, & Guyenet PG (2013). Cholinergic neurons in the mouse rostral ventrolateral medulla target sensory afferent areas. Brain Structure and Function, 218, 455–475. doi: 10.1007/s00429-012-0408-3 [PubMed: 22460939]

Suga N (2012). Tuning shifts of the auditory system by corticocortical and corticofugal projections and conditioning. Neuroscience & Biobehavioral Reviews, 36, 969–988. doi: 10.1016/j.neubiorev.2011.11.006 [PubMed: 22155273]

Sved AF, Ito S, & Yajima Y (2002). Role of excitatory amino acid inputs to the rostral ventrolateral medulla in cardiovascular regulation. Clinical and Experimental Pharmacology and Physiology, 29, 503–506. doi: 10.1046/j.1440-1681.2002.03663.x [PubMed: 12010199]

Takács VT, Freund TF, Nyiri G, 2013. Neuroligin 2 is expressed in synapses established by cholinergic cells in the mouse brain. PLoS One8, e72450. 10.1371/journal.pone.0072450 [PubMed: 24039767]

Tulloch AJ, Teo S, Carvajal BV, Tessier-Lavigne M, & Jaworski A (2019). Diverse spinal commissural neuron populations revealed by fate mapping and molecular profiling using a novel *Robo3* ^{Cre} mouse. Journal of Comparative Neurology, 527, 2948–2972. doi: 10.1002/cne.24720

Watanabe T, & Simada Z (1973). Pharmacological properties of cat's collicular auditory neurons. The Japanese Journal of Physiology, 23, 291–308. doi: 10.2170/jjphysiol.23.291 [PubMed: 4270927]

Whiteaker P, Jimenez M, McIntosh JM, Collins AC, & Marks MJ (2000). Identification of a novel nicotinic binding site in mouse brain using [^{125} I]-epibatidine. British Journal of Pharmacology, 131(4), 729–739. doi: 10.1038/sj.bjp.0703616 [PubMed: 11030722]

Xiong XR, Liang F, Zingg B, Ji X, Ibrahim LA, Tao HW, & Zhang LI (2015). Auditory cortex controls sound-driven innate defense behaviour through corticofugal projections to inferior colliculus. Nature Communications, 6, 7224. doi: 10.1038/ncomms8224

Xiong Y, Zhang Y, & Yan J (2009). The neurobiology of sound-specific auditory plasticity: A core neural circuit. Neuroscience & Biobehavioral Reviews, 33, 1178–1184. doi: 10.1016/j.neubiorev.2008.10.006 [PubMed: 19014967]

Yigit M, Keipert C, & Backus KH (2003). Muscarinic acetylcholine receptors potentiate the GABAergic transmission in the developing rat inferior colliculus. Neuropharmacology, 45, 504–513. doi: 10.1016/S0028-3908(03)00197-7 [PubMed: 12907311]

Zhang S, Qi J, Li X, Wang H-L, Britt JP, Hoffman AF, … Morales M (2015). Dopaminergic and glutamatergic microdomains in a subset of rodent mesoaccumbens axons. Nature Neuroscience, 18, 386–392. doi: 10.1038/nn.3945 [PubMed: 25664911]

Zheng QY, Johnson KR, & Erway LC (1999). Assessment of hearing in 80 inbred strains of mice by ABR threshold analyses. Hearing Research, 130, 94–107. doi: 10.1016/S0378-5955(99)00003-9 [PubMed: 10320101]

Highlights

- Four subtypes of GABAergic cells can be distinguished in the mouse inferior colliculus
- This may indicate conservation of these GABAergic subtypes across rodent species
- Cholinergic boutons form close associations with a majority of neurons in the mouse inferior colliculus, including both GABAergic and glutamatergic cells
- All four subtypes of GABAergic cells have close associations with cholinergic boutons
- This indicates widespread effects of acetylcholine on excitatory and inhibitory cells across the mouse inferior colliculus

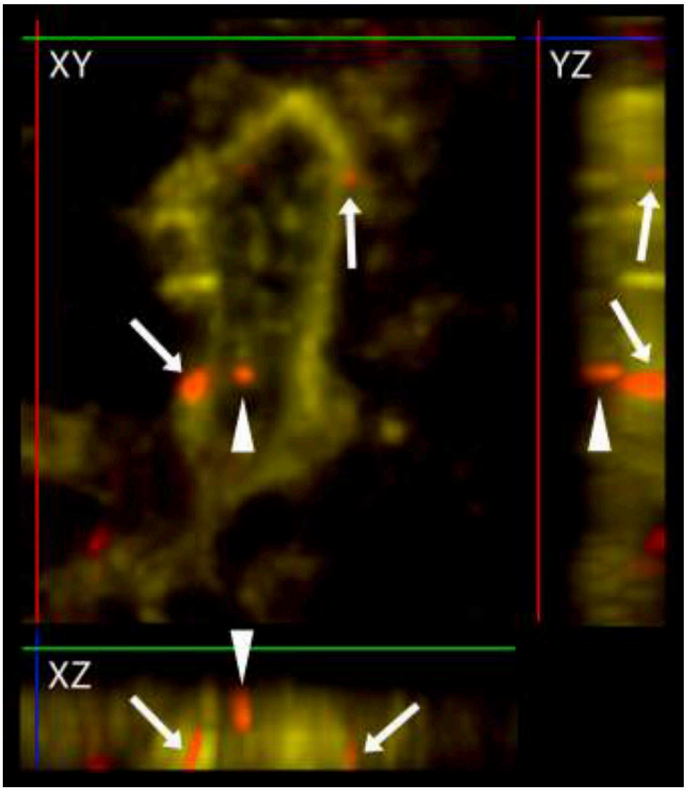

Figure 1. Examples of boutons in close apposition to an IC neuron

A z-stack image of a NeuN/Neurochrom-labeled neuron in the IClc (yellow), with ACh boutons (red) that are in close apposition (arrows) or not in close apposition (arrowheads) shown in three planes. The X plane is indicated by a green line, the Y plane is indicated by a red line, and the Z plane is indicated by a blue line. The XY image shows three red boutons in the vicinity of the labeled neuron. Rotation of the image stack to view YZ and XZ perspectives shows that the two ACh boutons indicated with arrows are in the same focal plane as the neuron and would be considered in close apposition with the neuron. The arrowhead-labeled bouton might be in contact with the neuron but the resolution in the Z-plane is not high enough to make this determination. Boutons like this were not classified as a “close apposition” even though such a conservative view likely lead us to underestimate the number of contacts.

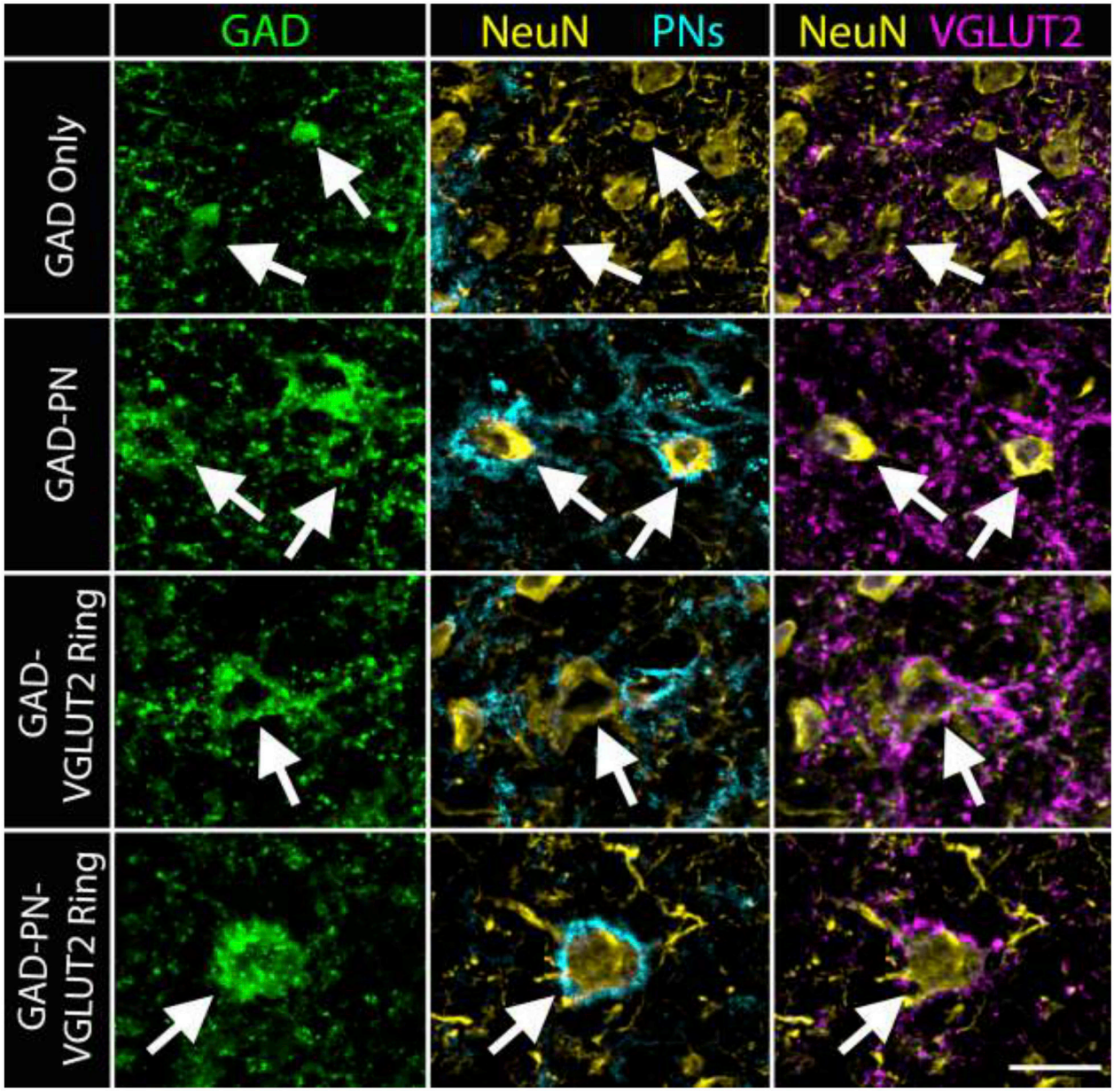

Figure 2. Four subtypes of GAD+ cells are present in the mouse IC.

Photomicrographs show GAD+ cells (green, first column) in the mouse IC and their association with PNs (cyan, second column) and rings of axosomatic VGLUT2+ terminals (VGLUT2 rings, magenta, third column). Cells were confirmed to be neurons with cocktail staining for NeuN and Neuro-Chrom ('NeuN', yellow, second and third columns). GAD+ cells could lack a PN and a VGLUT2 ring (GAD Only, white arrows, top row), could be associated with a PN, but no VGLUT2 ring (GAD-PN, white arrows, second row), could be associated with a VGLUT2 ring but not a PN (GAD-VGLUT2 ring, white arrow, third row), or could be associated with both a PN and a VGLUT2 ring (GAD-PN-VGLUT2 ring, white arrow, bottom row). Scale bar = 20 μm.

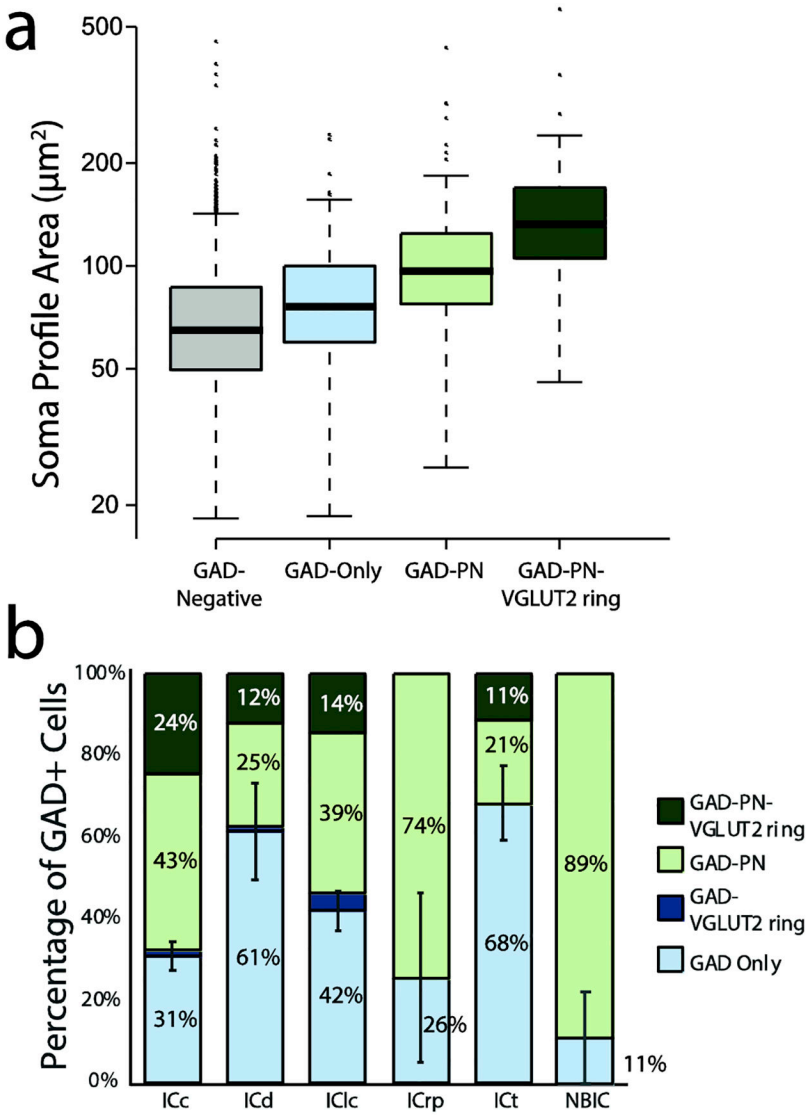

Figure 3. Subtypes of GAD+ cells differ in their average soma size and distribution across regions.

A. A boxplot depicting the median and range of soma profile areas for GAD-negative cells (gray), GAD Only cells (light blue), GAD-PN cells (light green), and GAD-PN-VGLUT2 ring cells (dark green). GAD-VGLUT2 ring cells were excluded from this analysis due to their low numbers (only four cells were observed across all regions and cases). GAD Only cells tended to have the smallest soma sizes, while GAD-PN-VGLUT2 ring cells tended to have the largest soma sizes. Note that the y-axis is logarithmic. n = 2273 neurons across three cases. **B.** A bar graph depicting the GAD+ population in each IC subdivision and intercollicular region analyzed. The GAD Only proportion is depicted in light blue, the GAD-VGLUT2 ring proportion is depicted in dark blue, the GAD-PN proportion is depicted in light green, and the GAD-PNN-VGLUT2 ring proportion is depicted in dark green. Error bars = SEM of the GAD Only population. n = 97 GAD Only cells, 106 GAD-PN cells, 4 GAD-VGLUT2 ring, and 45 GAD-PN-VGLUT2 ring cells across three cases.

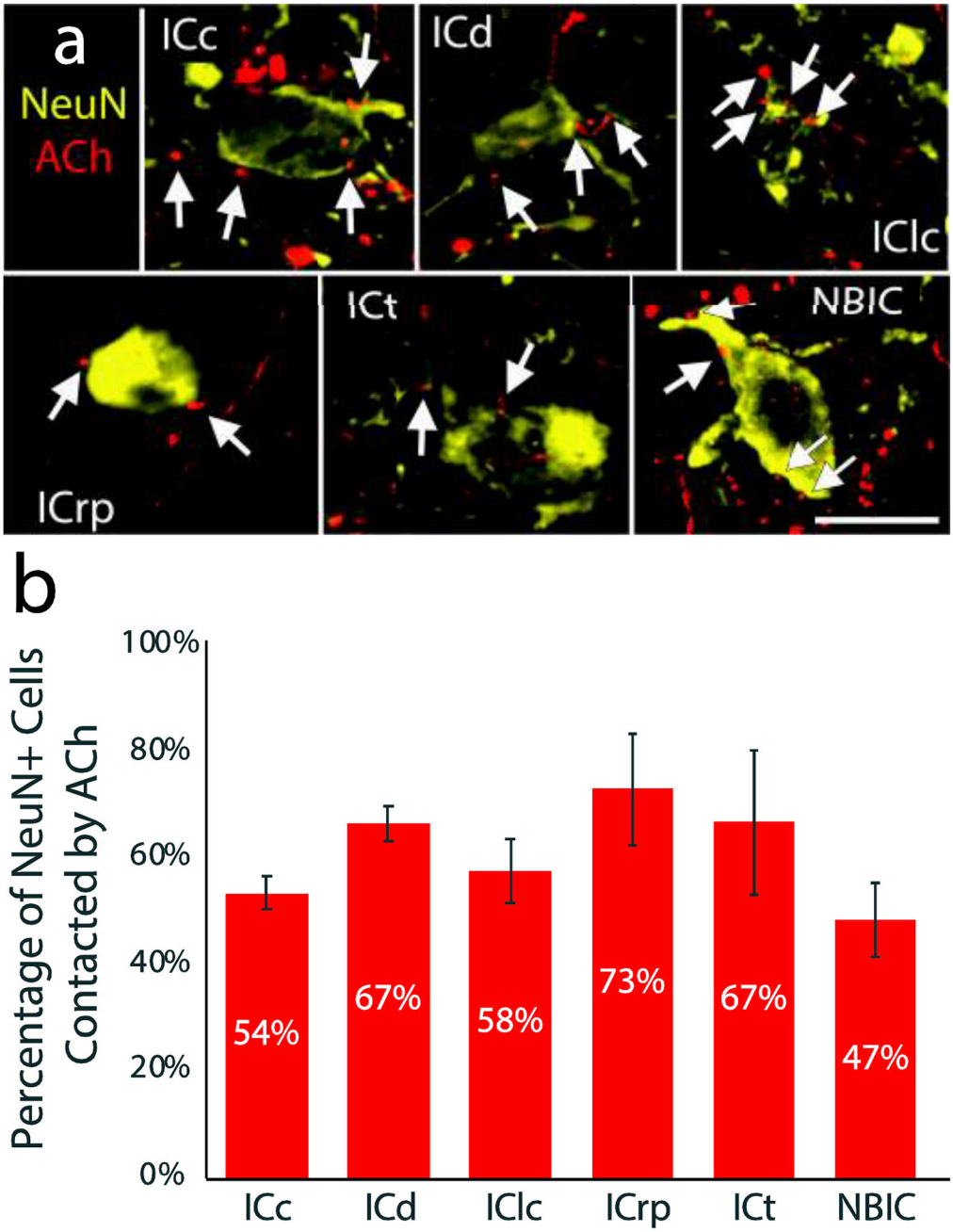

Figure 4. ACh axons form presumptive contacts on neurons across the IC and intercollicular regions.

A. Photomicrographs show neurons stained with an anti-NeuN/Neuro-Chrom cocktail ('NeuN', yellow). Axons filled with tdTomato (cholinergic axons, ACh, red) form presumptive contacts (arrows) with neurons in each region examined. Scale bar = 10 μm.

B. A bar graph shows the proportion of all NeuN+ neurons in the sample that receive presumptive cholinergic contacts in each area. There was no significant difference in the proportion of neurons associated with cholinergic contacts. Error bars = SEM.

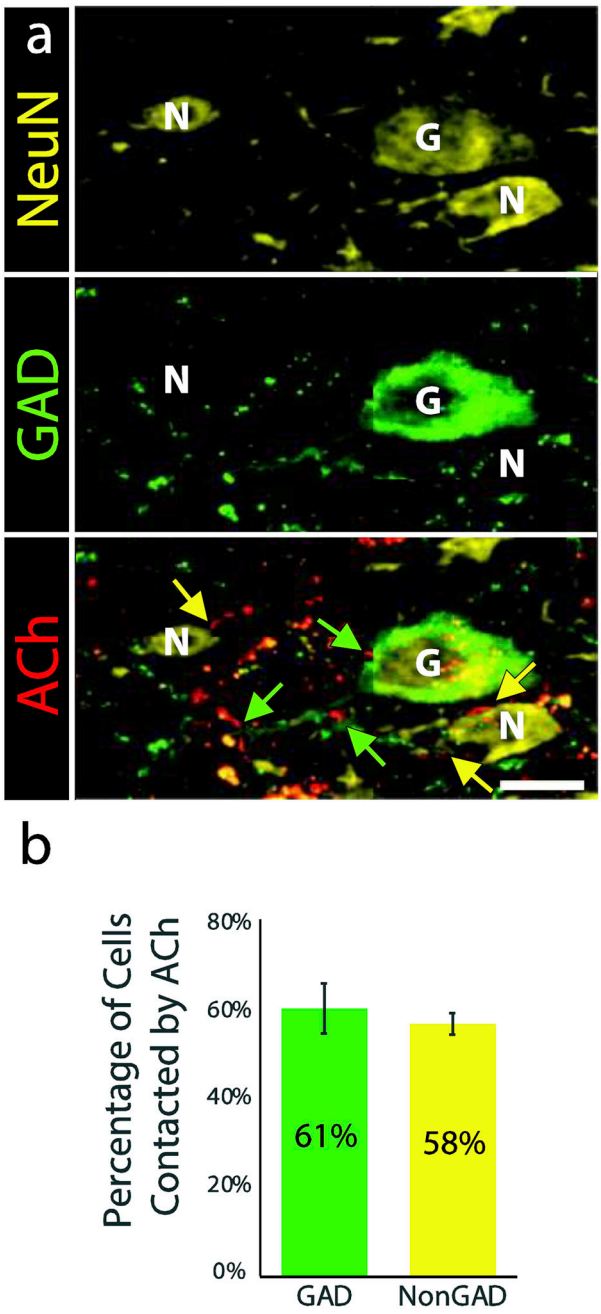

Figure 5. ACh axons form presumptive contacts with both GAD+ and GAD-negative neurons.

A. Yellow fluorescence (NeuN/Neuro-Chrom) shows 3 neurons. Staining with anti-GAD (green, middle panel) shows that one neuron is GAD+ ("G") while the other two are GAD-negative ("N"). Both neurotransmitter types receive presumptive contacts from tdTomato-labeled cholinergic axons (red, highlighted with yellow arrows on GAD-negative cells and green arrows on the GAD+ cell). Scale bar = 10 μm. **B.** A bar graph shows the proportions of GAD+ (green) and GAD-negative (yellow) neurons that received presumptive contact from cholinergic axons. There was no clear difference between the two types of cells. Error bars = SEM. n = 254 GAD+ and 2019 GAD-negative cells across three cases.

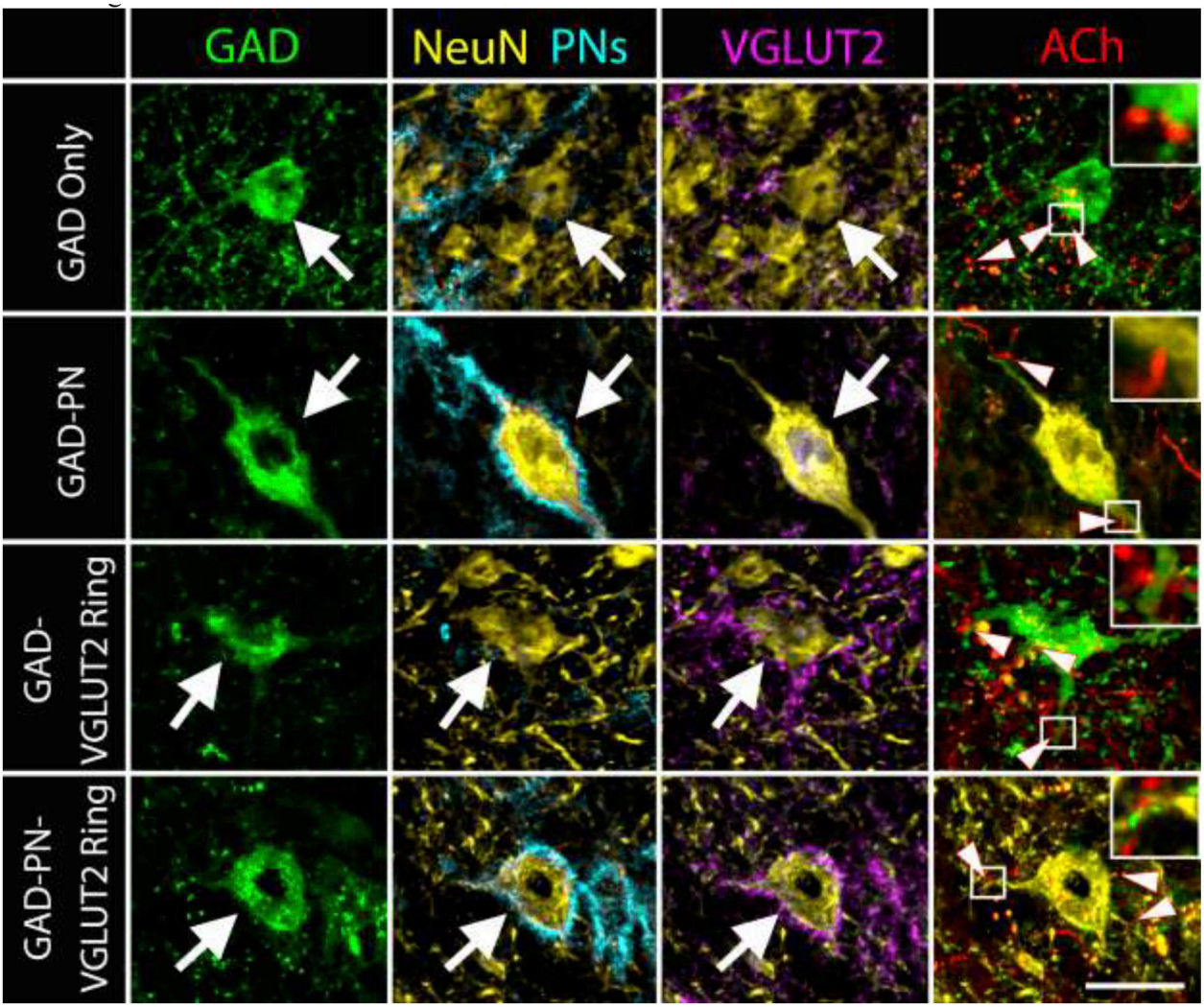

Figure 6. ACh axons form presumptive contacts with all four subtypes of GAD+ cells.
Photomicrographs show examples of each of the four subtypes of GAD+ cells (large arrows). In each example, tdTomato-filled cholinergic axons (red) make presumptive contacts with the soma or dendrites of the cells (arrowheads in the last column). Insets show enlargements of selected contacts (white boxes). Scale bar = 20 μm.

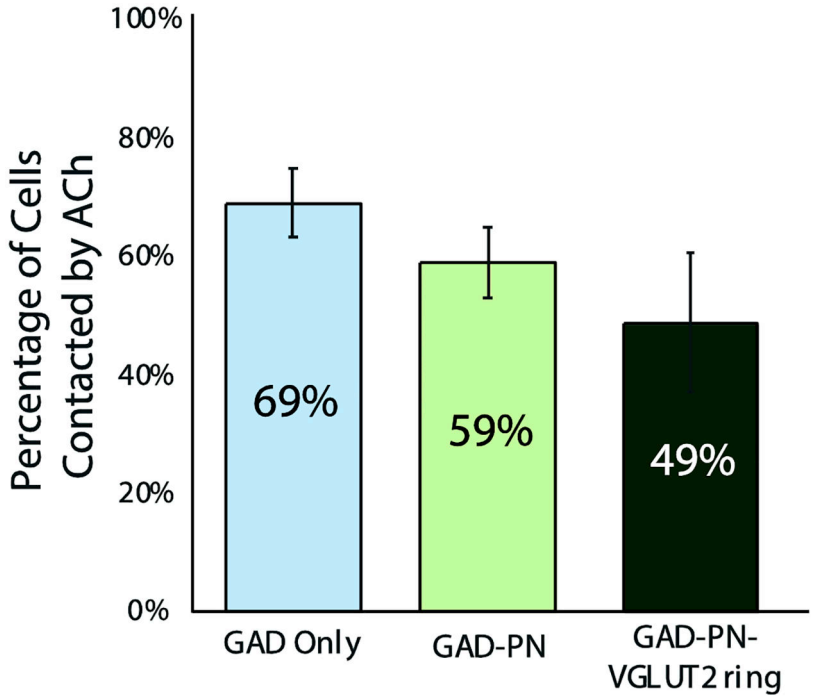

Figure 7. The subtypes of GAD+ cell are contacted in similar proportions.

A bar graph shows the proportion of the three prominent GAD+ subtypes that received presumptive contact from cholinergic axons. Error bars = SEM. n = 97 GAD Only cells, 106 GAD-PN cells, and 45 GAD-PN-VGLUT2 ring cells across three cases. Note that the GAD-VGLUT2 ring group is excluded from the graph because of the small number of such cells (4 in the sample). Despite the small number, two of these cells appeared to be contacted by cholinergic axons.

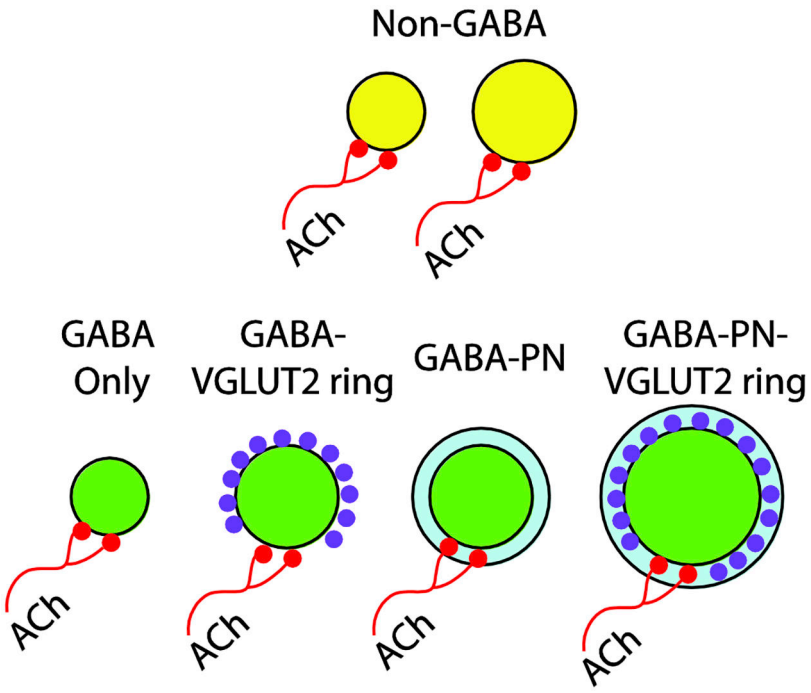

Figure 8. Summary

A schematic diagram depicting cell populations in the mouse IC. Non-GABAergic cells (yellow) and GABAergic cells (green) both receive input from cholinergic axons (red). All four subtypes of GABAergic cells are contacted, including those surrounded by PNs (light blue) and those surrounded by rings of axosomatic VGLUT2+ terminals (purple).